THE ASTROPHYSICAL JOURNAL, 372:185–193, 1991 May 1

IRAS DETECTION OF VERY COLD DUST IN THE LYNDS 134 CLOUD COMPLEX

R. J. LAUREIJS[1]
Infrared Processing and Analysis Center, Jet Propulsion Laboratory, California Institute of Technology, Pasadena, CA 91125
F. O. CLARK
Geophysics Laboratory, OPB Hanscom Air Force Base, MA 01731
AND
T. PRUSTI
Laboratory for Space Research and Kapteyn Astronomical Institute, P.O. Box 800, 9700 AV Groningen, The Netherlands
Received 1990 August 20; accepted 1990 October 12

ABSTRACT

We have analyzed *IRAS* maps at 60 and 100 μm of the complex of dark clouds containing L134, L183 and L1780. Regions were found that are bright at 100 μm but not detected at 60 μm. These regions exhibit high optical opacities and are associated with the dark clouds. The 60 μm surface brightness is observed to decline in a narrow transition layer surrounding the cloud centers. In the outer environs the ratio I_{60}/I_{100} has a nearly constant value of 0.2. The absence of 60 μm emission yields an upper limit of 15 K for the temperature of the dust, assuming λ^{-1} dust emissivity. We have mapped the 60 μm deficient regions using the quantity $\Delta I_{100} = I_{100} - I_{60}/\Theta$, where Θ is the ratio I_{60}/I_{100} in the outer diffuse regions. We have found a linear correlation between ΔI_{100} and both ^{13}CO column density and blue extinction. The analysis suggests that the diffuse component of the cloud has been subtracted when constructing ΔI_{100}, and that ΔI_{100} is tightly correlated with molecular material with densities in excess of $n(H_2) = 10^3$. We have derived an upper limit for the mass absorption coefficient of dust at 100 μm of 4.8 g cm^{-2}. This limit is consistent with earlier determinations. The sudden drop in the 60 μm emission can only be explained when assuming a separate grain component at 60 μm that undergoes a change in properties in a narrow transition region. We infer that condensation of a thin mantle on the grains in the transition layer can explain the observed infrared properties.

Subject headings: infrared: sources — interstellar: grains — nebulae: individual (Lynds 134)

1. INTRODUCTION

The dust responsible for the extinction and polarization at optical and near-infrared wavelengths (hereafter referred to as "classical grains") is assumed to be well-mixed with hydrogen gas either in atomic or molecular form (Bohlin, Savage, & Drake 1978). This property combined with the transparency of dense regions at far-infrared wavelengths makes thermal radiation of dust a potential tool to probe obscured mass concentrations in dense clouds. The biggest source of uncertainty is the assumed composition and shape of the particles giving rise to the infrared emission (Mathis & Whiffen 1989). A necessary parameter to describe the emission is the temperature of the particles.

Theoretical studies of classical grains predict temperatures below 20 K in the diffuse and dense interstellar medium for various proposed grain materials (Werner & Salpeter 1969; Spencer & Leung 1978; Lee & Rogers 1989; Draine & Lee 1985; Draine 1990). For instance, Draine & Lee (1985) derive temperatures of about 19 K for graphite, and about 15 K for silicate particles heated by the interstellar radiation field. In denser regions the temperature must be lower due to the attenuation of the radiation field. Unfortunately, direct observational evidence for cold dust from the measurement of its far-infrared spectral distribution is based on observations of only a few objects (Keene 1981). This scarcity is due to the relative weakness of the emission and its large extension with respect to the possible chop-throw of available telescopes. The lack of observational evidence is unfortunate since a precise measurement could constrain grain models (Hildebrand 1983). Indirect evidence for dust as cold as 18 K has been obtained by comparing column density estimates with the infrared surface brightness at a single wavelength (Terebey & Fich 1987), or by modeling the spectral distribution in the direction of warm dusty sources in which the cold dust component is likely to contribute to the far-infrared emission (Mathis, Mezger, & Panagia 1986).

The vast amount of data obtained by *IRAS* has introduced an unexpected controversy on the reality of cold dust in the diffuse interstellar medium: whereas comparison of the 100 μm emission with atomic hydrogen column density indicates grain temperatures of about 18 K, the color temperature derived from the ratio of the emission in the 60 and 100 μm bands yields temperatures of 23–28 K (Terebey & Fich 1986). The discrepancy can be explained by assuming the presence of an additional emission component in the 60 μm band (see review by Cox & Mezger 1989). The relationship between the 60 and 100 μm emission has been studied in detail in the diffuse interstellar medium (Boulanger & Pérault 1988) and in a number of low opacity clouds at high latitude (Laureijs, Chlewicki, & Clark 1988; Heiles et al. 1988).

To ascertain more precisely the behavior of the far-infrared emission at 60 and 100 μm in connection with the cold dust controversy, we analyze in this paper *IRAS* maps of a high-latitude cloud complex at $l = 4°$, $b = 36°$. The complex contains the dark clouds L134 and L183 (the latter is often referred to as L134N) which are known to contain dense molecular cloud cores (Benson & Myers 1989) and L1780. Photometric

[1] NRC Fellow.

observations by Franco (1989) indicate that the cores are embedded in an envelope of several degrees in extent, which has a visual opacity less than 1 mag. The distance to the complex is only 100 pc (Mattila 1979; Franco 1989) and no star formation activity has been reported, making it an appropriate site to study infared emission properties of both dense and diffuse material.

In § 2 we describe the processing of the infrared data. In § 3 the emission at 60 and 100 μm is analyzed and compared with other observations. Interpretations of the results in terms of grain properties are discussed in § 4. In § 5 we present the implications of this study.

2. INFRARED DATA

The *IRAS* data at 60 and 100 μm were co-added into images according to a procedure presently available as a standard *IRAS* product (BIGMAP 2). Before co-addition, the individual detector scans at 60 and 100 μm were convolved to a common in-scan resolution of 5′. A zodiacal emission model was subtracted generating a linear baseline in each detector scan. To correct for possible distortions in the image due to baseline discrepancies between scans ("stripes"), an iterative procedure for co-addition has been applied (Kester 1989). During each iteration, differences between the average map level and a detector scan were minimized by subtracting a linear baseline from each scan. On scales less than a degree, the images are free from stripes at typical intensity levels of less than 0.2 MJy sr^{-1} at both 60 and 100 μm. On larger scales, background discrepancies between the different *IRAS* surveys may result in stripes of several degrees width with a brightness amplitude of about 1 MJy sr^{-1}. The zero brightness level in the maps with respect to the cloud complex is arbitrary.

3. ANALYSIS

3.1. *Cloud Profiles*

A comparison between the surface brightness at 60 and 100 μm (in units of MJy sr^{-1}, hereafter denoted by I_{60} and I_{100}, respectively) towards L134, L183, and L1780 is given in Figure 1 where three different slices through the clouds are displayed. As shown in Figure 1, I_{60} has been divided by a factor Θ which is defined as

$$\Theta = I_{60}/I_{100} , \quad (1)$$

measured at low 100 μm brightness levels.

The slices in Figures 1*a* and 1*b* exhibit a one-to-one correspondence between I_{60} and I_{100} at low brightness levels. The constancy of the ratio I_{60}/I_{100} makes an accurate determination of Θ possible. We obtain $\Theta = 0.21 \pm 0.01$ by varying the brightness ratio until the best match between the 60 and 100 μm brightness is achieved, the quoted uncertainty is the estimated probable error. At certain positions along the slices a "decoupling" between the emission in the 60 and 100 μm bands occurs: while I_{100} continues to increase, I_{60} exhibits either a decline or remains constant. In Figure 1*c* we have included a profile of the translucent cloud L1780 with a peak extinction of $A_B = 4$ mag (Mattila 1979), showing the same variation seen in the dense clouds L183 and L134 (peak extinction $A_B > 10.3$ mag). A straightforward ratio of I_{60} and I_{100} in the center of L1780 would indicate a small color variation. Figure 1*c*, however, suggests a sudden decline in 60 μm emission relative to the 100 μm emission, which is confined to a small region embedded in the cloud.

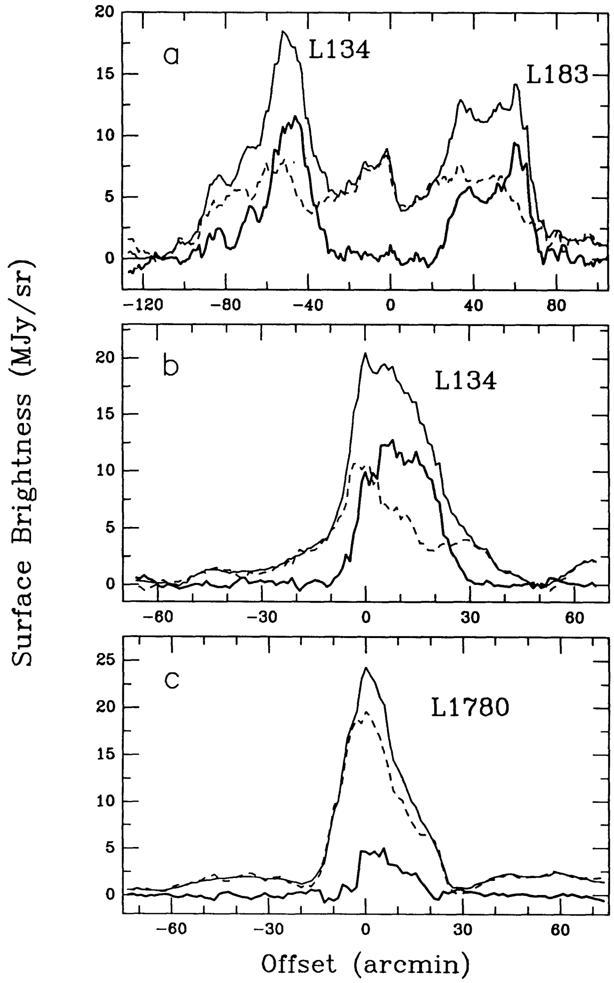

FIG. 1.—Profiles of the surface brightness at 60 and 100 μm. The emission of 60 μm (*dashed lines*) has been divided by $\Theta = 0.21$ for comparison with the 100 μm profiles (*thin solid lines*). The profiles of ΔI_{100} obtained by subtracting the scaled 60 μm emission from I_{100} is indicated by the thick solid lines. (*a*) a slice through both L183 and L134, and extends from $\alpha(1950) = 15^h52^m10^s$, $\delta(1950) = -2°6'32''$ to $\alpha(1950) = 15^h50^m18^s$, $\delta(1950) = -5°51'27''$; (*b*) profile of L134 [from $\alpha(1950) = 15^h55^m39^s$, $\delta(1950) = -5°11'26''$ to $\alpha(1950) = 15^h47^m45^s$, $\delta(1950) = -4°11'28''$]; (*c*) profile of L1780 [from $\alpha(1950) = 15^h33^m20^s$, $\delta(1950) = -7°54'26''$ to $\alpha(1950) = 15^h40^m19^s$, $\delta(1950) = -6°10'28''$].

The profiles presented in Figure 1 clearly show the existence of regions in the L134 complex where the 60 μm emission is much weaker with respect to its surroundings. We derived the *excess* 100 μm profile, ΔI_{100}, according to the relationship

$$\Delta I_{100} = I_{100} - I_{60}/\Theta . \quad (2)$$

The resulting profiles of ΔI_{100} are included in Figures 1*a*–1*c*. They show a number of remarkable properties. First, the baselines are flat. The rms noise away from the features is about 0.3 MJy sr^{-1}, close to the value of the expected instrumental noise. This demonstrates that the ratio I_{60}/I_{100} is constant except in confined regions in the L134 cloud complex. Second, ΔI_{100} rises steeply on the flanks of the cloud cores. The rise occurs over a distance less than 10′, indicating that the 60 μm emission declines in a narrow cloud layer that is possibly not resolved by *IRAS*. Third, the peaks at I_{100} and also the minima in the ratio I_{60}/I_{100} do not always coincide with the maxima seen in ΔI_{100}.

3.2. *Modeling of the L134 Profile*

To quantify the actual change in the 60 μm emission with respect to the 100 μm emission, the following geometrical model has been constructed. We consider a spherical cloud with an outer radius R. In the outer parts of the cloud, the 100 μm emission per unit volume, F_{100}, decreases with an r^{-2} dependency where r is the distance to the cloud center. This assumption is based on the observation that 100 μm profiles of high-latitude clouds closely follow an r^{-2} dependency in the outer parts (Laureijs, Mattila, & Schnur 1987; Laureijs et al. 1989). In the central regions of the cloud out to a radius a, the 100 μm emission is considered to be uniform. Thus $F_{100}(r)$ can be written according to

$$\begin{aligned} F_{100}(r) &= Cr^{-2} \quad a < r < R \\ &= Ca^{-2} \quad 0 < r < a , \end{aligned} \tag{3a}$$

where C is a scaling constant. To model the 60 μm profiles, we assume that the emission per unit volume at 60 μm is proportional to that at 100 μm. In the outer parts of the cloud we assume the ratio F_{60}/F_{100} equal to θ, in accordance with the observed constancy of I_{60}/I_{100}. The sudden drop in the 60–100 μm ratio has been modeled by assuming an inner region with a radius b where the ratio F_{60}/F_{100} is lower by a factor f. The 60 μm profile is described by

$$\begin{aligned} F_{60}(r) &= C\theta r^{-2} \quad b < r < R \\ &= C\theta f r^{-2} \quad a < r < b \\ &= C\theta f a^{-2} \quad 0 < r < a . \end{aligned} \tag{3b}$$

Radius a is obtained from the fit to the observed profile at 100 μm. The 60 μm profile is subsequently matched by adjusting the parameters b and f. The value for θ has been taken from the observations in the previous section.

Model fits to the profile of L134 are displayed in Figure 2. The center of the profile corresponds to the maximum value of ΔI_{100} (Fig. 1*b*). The fitted profiles have been smeared with a 5′ wide boxcar function to mimic the resolution of the *IRAS* observations. We allowed different fitting parameters for the eastern and western half to account for the observed asymmetry in the 60 μm profile.

The good match between the model and the observed 60 μm emission confirms that the decline in the 60 μm emission occurs in a narrow cloud layer. The correspondence between the calculated and the observed emission both at 60 and 100 μm in Figure 2 shows that the emission model is adequate to estimate the decline in the 60 to 100 μm ratio.

The values for f derived from the L134 profile are $f < 0.05$ and $f = 0.15$ for the eastern and western half, respectively. The small values of f support the validity of the subtraction method according to equation (2). We adopt an upper limit of $f < 0.15$ which corresponds to an actual 60–100 μm ratio of $f \cdot \Theta < 0.03$ where $\Theta = 0.21$. The ratio provides an upper limit for the temperature of the grains responsible for the cloud core emission. Considering two different models for the infrared absorption coefficient Q_{abs} which determines the far-infrared emissivity, we obtain

$$\begin{aligned} T_d &< 15.1 \text{ K} \quad Q_{abs} \propto \lambda^{-1} \\ T_d &< 13.8 \text{ K} \quad Q_{abs} \propto \lambda^{-2} . \end{aligned} \tag{4}$$

These values have been corrected for the shape of the *IRAS* transmision functions.

3.3. *Infrared Images*

Images of I_{100} and ΔI_{100} of a large part of the cloud complex are presented in Figures 3*a* and 3*b*, respectively. As expected from the analysis given in the previous section, nearly all of the extended infrared cirrus emission (Low et al. 1984) in Figure 3*a* has disappeared in Figure 3*b*, down to a surface brightness level of $\Delta I_{100} < 1$ MJy sr^{-1}. Remaining are isolated

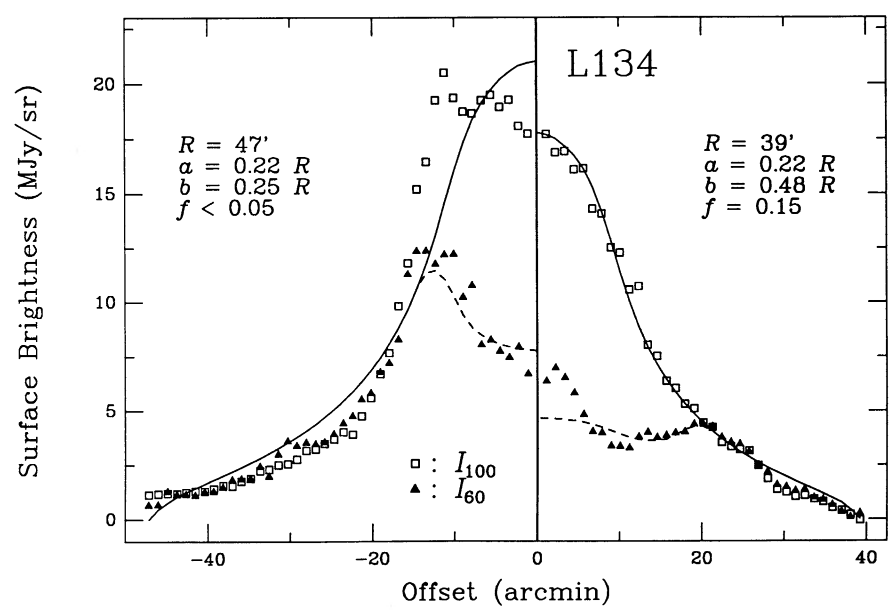

FIG. 2.—Geometrical model of the 60 and 100 μm emission in L134 to quantify the variation in the 60–100 μm ratio in the interior of the cloud. The eastern (*left panel*) and western half of the slice have been fitted separately in order to account for the observed asymmetry. The lines represent the best fits; *solid lines*: 100 μm emission, *dashed lines*: 60 μm emission. See § 3.1 for a description of the fitting parameters.

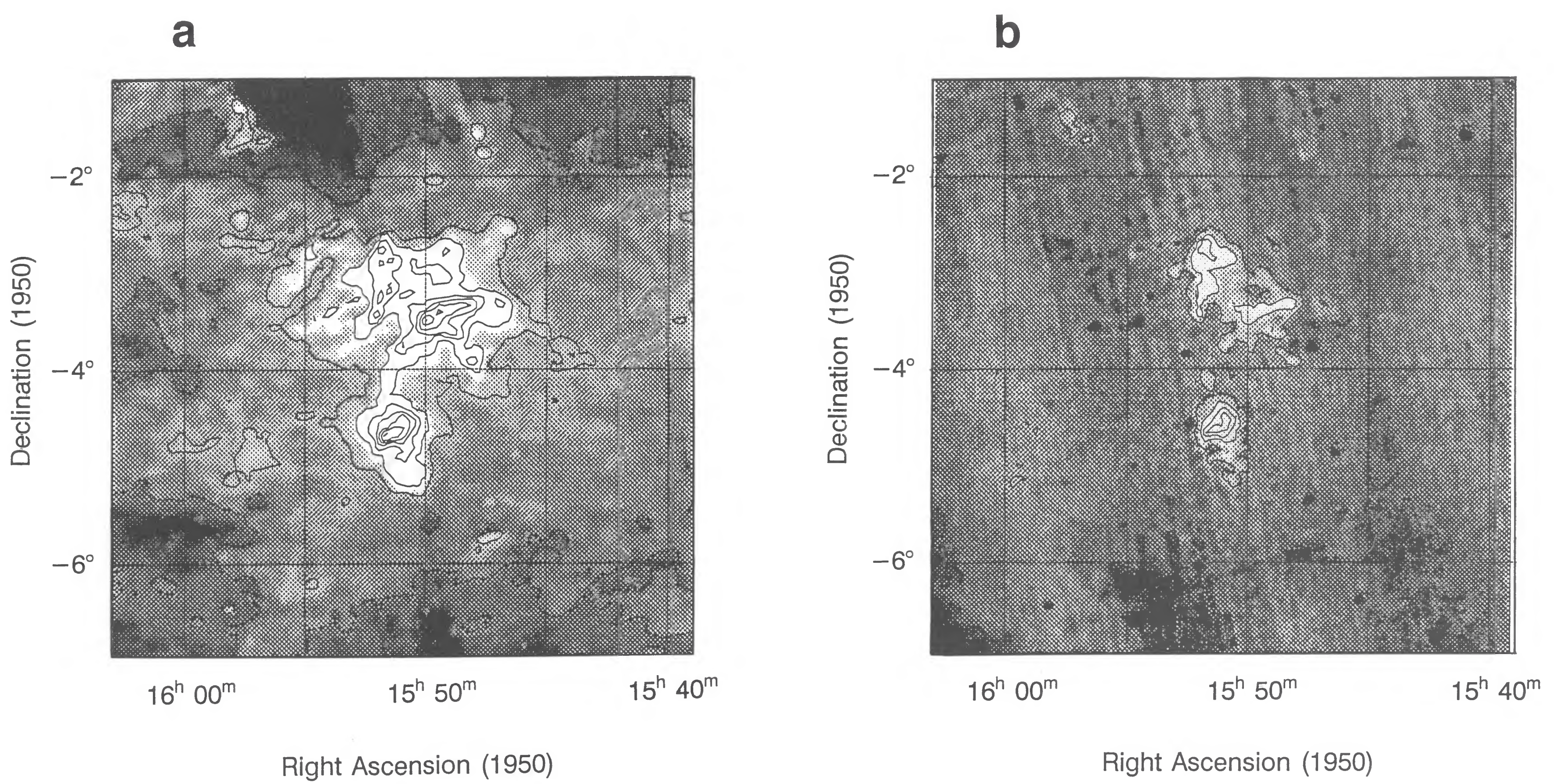

FIG. 3.—L134 complex of molecular clouds before (*a*) and after (*b*) subtraction of I_{60}/Θ from I_{100}. An additional flat-fielding has been applied by fitting a tilted plane through the lowest regions in the maps. The contours correspond to levels of -1 MJy sr^{-1} (*dashed lines*) and 2, 5, 8, ... MJy sr^{-1} (*solid lines*). The positions of the clouds are: L183 at $\alpha(1950) = 15^h51^m$, $\delta(1950) = -2°43'$; L134 at $\alpha(1950) = 15^h51^m$, $\delta(1950) = -4°30'$; L1780 at $\alpha(1950) = 15^h37^m$, $\delta(1950) = -7°5'$ lies outside the map. Strong point sources at 60 μm show up as negative sources in the map of ΔI_{100}.

regions associated with the dark clouds. The map of ΔI_{100} shows a good correspondence with the features seen in the 6 cm rotational transition of formaldehyde (H_2CO $1_{10} \rightarrow 1_{11}$) observed by Clark & Johnson (1983). Most striking is the change in appearance of L134. Two peaks appear in ΔI_{100} of which the brightest is located in the NW part of the cloud. This spot is coincident with the position of the cloud core which has been detected in several molecules (Mattila, Winnberg, & Grasshoff 1979) including ammonia (Benson & Myers 1989).

The peak ΔI_{100} in the direction of L183 coincides with the ^{13}CO peak mapped by Snell (1981) and Swade (1989) and it is close to the eastern CS condensation mapped by Snell, Langer, & Frerking (1982) but is not coincident with. It is located about 7′ east of the position of the strong ammonia core (Ungerechts, Walmsley, & Winnewisser 1981; Swade 1989). Observations of several molecular lines have shown that the ammonia core is associated with a high density region [$n(H_2) > 10^5$; Swade 1989]. The presence of such a region not detected at 100 μm indicates that the 100 μm emission is sensitive to a limited range in volume density in the absence of internal heating sources.

3.4. *Comparison with Column Density Estimates*

We have taken star counts for L134 from Mattila (1979) and converted these into blue extinction, A_B, according to the description given by Mattila (1986). The infrared maps have been regridded to match the 3′ × 3′ star count reseau in the extinction map. The resulting pixel-to-pixel correlation diagrams of I_{100} and ΔI_{100} versus blue extinction are presented in Figures 4*a* and 4*b*, respectively. The formal uncertainties in A_B derived from the star count statistics are illustrated by the error bars at the bottom of Figure 4*b*. The margins of error in A_B are not symmetrical and grow larger with increasing A_B.

Although the dynamic range of ΔI_{100} is smaller than that of I_{100} by about 30%, the correlation coefficient in Figure 4*b* is 0.75 and is not significantly different from the correlation coefficient in Figure 4*a* (=0.72). Apparently, the subtraction of the 60 μm component does not change the scatter but only the slope in the distribution of ΔI_{100} versus A_B. The formal uncertainties in A_B (depicted in Fig. 4*b*) can explain most of the scatter in Figures 4*a* and 4*b*.

For extinction values in excess of 5 mag, there is an indication that the ratio $\Delta I_{100}/A_B$ becomes smaller. However, this trend is predominantly due to the lower limits in the star counts and has little quantitative significance. We included in Figure 4 the relationship between I_{100} and A_B derived from the Galactic cosecant fits for I_{100} and atomic hydrogen N_H obtained by Boulanger & Perault (1988). To convert their observations to the quantities used by us, we adopted a ratio of total-to-selective extinction R_V of 3.1 (Savage & Mathis 1979) and the N_H versus A_V relationship given by Bohlin et al. (1978). The data points in Figure 4*a* for which $A_B < 2$ mag show a scatter along the N_H versus I_{100} relationship. In Figure 4*b* a large number of these data points has been shifted to a constant level of $\Delta I_{100} = \sim 8.5$ MJy sr^{-1}. The removal of the scatter around the I_{100} versus N_H relationship suggests that ΔI_{100} is not associated with atomic hydrogen.

Correlation diagrams in which I_{100} and ΔI_{100} are compared with a molecular column density estimate, $N(^{13}CO)$, are presented in Figure 5. The molecular data have been taken from Snell (1981) who observed ^{12}CO and ^{13}CO in the direction of L183 and used a large velocity gradient model to convert the ^{13}CO data to column densities. The data presented in Figure 5

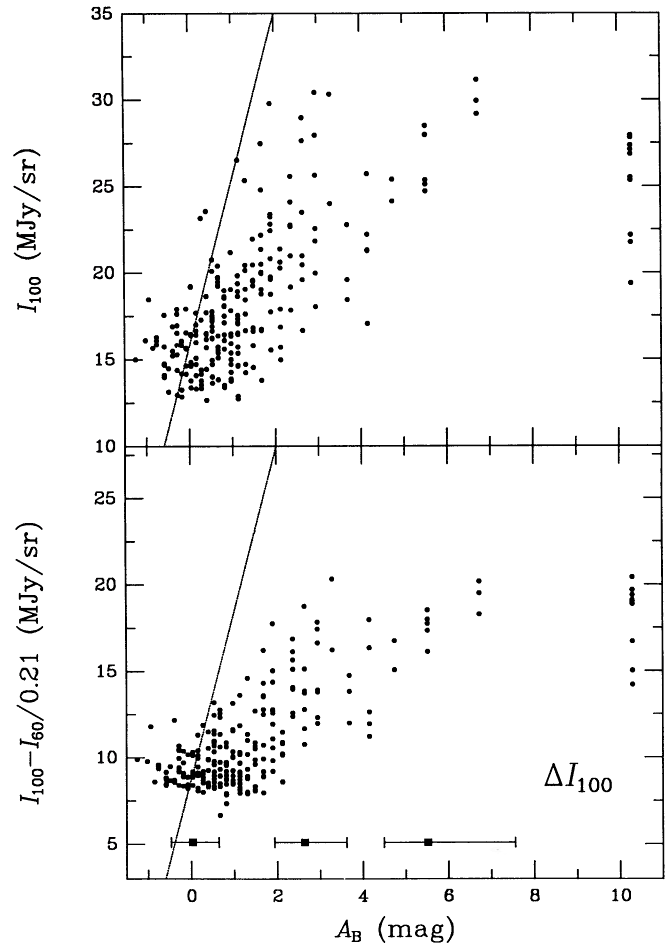

FIG. 4.—Comparison of I_{100} (*a, upper panel*) and ΔI_{100} (*b, lower panel*) with blue extinction. The quantity A_B has been taken from Mattila (1979, 1986). The lines present the relationship between I_{100} and A_B derived from the relationship between I_{100} and N_H obtained by Boulanger & Perault (1988). The error bars in Fig. 4*b* denote the formal errors derived from Poisson statistics of the star counts.

have not been corrected for the differences in beam size between the ^{13}CO (2′.3 resolution) and infrared (5′ resolution) observations because of the sparse CO sampling. Figure 5*a* clearly exhibits a low correlation between I_{100} and $N(^{13}CO)$ and there is a suggestion for a nonlinear relationship. After subtraction of I_{60}/Θ, the correlation coefficient has improved from 0.55 (Fig. 5*a*) to 0.79 in Figure 5*b*. Moreover, in Figure 5*b* there is no evidence for a nonlinear relationship between ΔI_{100} and $N(^{13}CO)$. Since part of the scatter can be attributed to the difference in spatial resolution between the observations, we expect a tighter correlation between $N(^{13}CO)$ and ΔI_{100} in L183 if the CO data were fully sampled and smoothed.

Assuming linear relationships and both A_B and $N(^{13}CO)$ to be the independent *x*-variables, we obtain from least-squares fits the following slopes:

$$I_{100}/A_B = 1.99 \pm 0.12 \quad \text{MJy sr}^{-1}\ \text{mag}^{-1}\ , \tag{5a}$$

$$\Delta I_{100}/A_B = 1.44 \pm 0.08 \quad \text{MJy sr}^{-1}\ \text{mag}^{-1}\ , \tag{5b}$$

$$\Delta I_{100}/N(^{13}\text{CO}) = (0.66 \pm 0.07) \times 10^{-15} \quad \text{MJy sr}^{-1}\ \text{cm}^{-2}\ . \tag{5c}$$

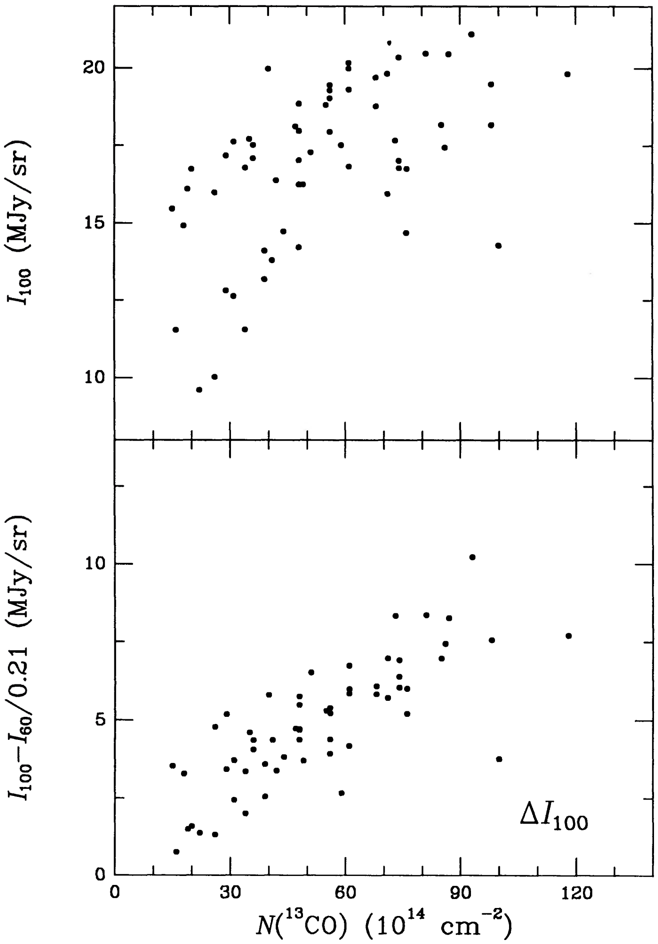

FIG. 5.—Comparison of I_{100} (*a, upper panel*) and ΔI_{100} (*b, lower panel*) with ^{13}CO column density. The ^{13}CO were taken from Snell (1981).

The lower limits in the extinction have been ignored in the calculation. We did not calculate the slope in I_{100} versus $N(^{13}CO)$ because of the poor correlation and nonlinear appearance of the distribution. The numbers presented in equations (5a) and (5b) are at the lower end of the values previously found in diffuse regions as well as in dark clouds (see e.g., Heithausen & Mebold 1989).

Dividing results (5b) and (5c), we obtain $N(^{13}CO)/A_V = (2.9 \pm 0.3) \times 10^{15}$ cm^{-2} mag^{-1}. This ratio is close to the value recently obtained by Dickman & Herbst (1990) who find a slope $N(^{13}CO)/A_V = (2.16 \pm 0.12) \times 10^{15}$ cm^{-2} mag^{-1} from the analysis of ^{13}CO and star counts at $\lambda = 8000$ Å in the ρ Oph complex. Our value does not deviate from other determinations of the ratio (Bachiller & Cernicharo 1986). The agreement suggests that ΔI_{100} is an independent column density estimate which is very closely associated to ^{13}CO emission. In contrast, I_{100} includes additional emission associated with diffuse parts in the clouds. Our result also implies that the gas-to-dust ratio as well as the temperature is uniform for the grains causing ΔI_{100} in both L134 and L183.

The temperature estimate given in equation (4) and the relationships between infrared emission and column density provide an upper limit for the mass absorption coefficient of the dust at 100 μm. Adopting the same notations as presented in Hildebrand (1983), the mass absorption coefficient can be estimated from the relationship

$$C_{100} = B_\nu(T_d)[I_{100}/A_B]^{-1}[N(H + H_2)/A_V] \times [R_V/(R_V + 1)]m_H \mu , \quad (6)$$

where B is the Planck function, m_H is the mass of a hydrogen atom, and μ (=1.4) is the ratio total gas mass to hydrogen mass. Using equation (5b), $N(H + H_2)/A_V = 1.9 \times 10^{21}$ cm^{-2} mag^{-1} (Bohlin et al. 1978), and $R_V = 3.1$ (Savage & Mathis 1979) we arrive at the following coefficients:

$$C_{100} < 4.8 \text{ g cm}^{-2} \quad (Q_{abs} \propto \lambda^{-1} \text{ temperature estimate})$$
$$C_{100} < 1.9 \text{ g cm}^{-2} \quad (Q_{abs} \propto \lambda^{-2} \text{ temperature estimate}) . \quad (7)$$

The validity of equation (6) relies upon the assumption that the 100 μm emission is due to grains emitting at a single temperature and that Q_{abs} of these grains is a power law of wavelength. However, the upper limits in equation (7) are still valid if the dust contained an additional grain component at a temperature lower than those found in equation (4).

The standard values of $N(H + H_2)/A_V$ and R_V used by us are in principle only applicable to dust in diffuse clouds. An alternative estimate of C_{100} can be obtained by considering the extinction properties towards ρ Oph, which refer to denser regions. From the near-infrared photometry carried out by Whittet & van Breda (1979) we adopt $A_V = 1.95$ mag and $R_V = 4.1$; the total column density is given in de Boer et al. (1986): $N(H + H_2) = 4.0 \times 10^{21}$ cm^{-2}. Inserting these values in equation (6) we derive limits that are only 7% lower than those presented in equation (7). Apparently, the lower ratio $N(H + H_2)/A_V$ and the higher value of $R_V/(R_V + 1)$ towards ρ Oph largely cancel each other out in equation (6).

Result (7) depends only weakly upon other assumptions involving the optical properties of grains. The uncertainties in the adopted value of R_V affects C_{100} only marginally. The presence of optical extinction in equation (6) (A_B and A_V) is necessary to relate the emission at 100 μm to a total mass estimate. We therefore believe that the values presented in (7) are robust upper limits for C_{100}. The difference between the two estimates in (7) gives an impression of the extent to which variations in temperature can modify C_{100}. Our upper limits of C_{100} are very close to the generally adopted empirical value quoted by Hildebrand (1983) of 4 g cm^{-2} which is at best accurate within a factor of 2. The number given by Hildebrand (1983) has been derived from observations of dense material in reflection nebulae.

4. INTERPRETATION AND DISCUSSION

4.1. *Properties of the* 60 μm *Deficient Regions*

The brightness profiles analyzed in § 3.1 show a dramatic decrease in the 60–100 flux ratio in a narrow layer surrounding the cloud. The 60 μm emission tends to fade at different values of I_{100}. Due to this property, I_{60} versus I_{100} pixel-to-pixel correlation diagrams will yield a larger dispersion at higher brightness levels, obscuring the sudden changes seen in the slices of Figure 1. Therefore, such correlation diagrams and also 60–100 brightness ratio maps should be interpreted with caution, especially in regions containing dense clouds.

The difference in morphology between ΔI_{100} and maps of several high-density probes (§ 3.3) suggest the presence of cloud condensations not detected at 100 μm. This is possible if the temperature of the dust is several degrees lower than the upper limits given in (2). Consequently, the temperature in these regions furnishes a lower limit for the temperature of the dust associated with ΔI_{100}. A temperature estimate can be obtained by assuming that at high densities the dust is in thermal equilibrium with the gas (Goldsmith & Langer 1978). Such a coupling implies that the dust temperature should be identical to the gas kinetic temperature T_k. A method to determine T_k is by measuring transitions of ammonia with equal values of levels J and K (Goldsmith 1987). From ammonia (J, K) = (1, 1) and (2, 2) line observations, Benson & Myers (1989) deduce kinetic temperatures of 9.0 and 9.5 K for L134 and L183, respectively. The value for L183 is consistent with the determination of Ungerechts et al. (1980), but is a few degrees lower than $T_k = 13$ K obtained by Swade (1989). In either case, these observations bracket the temperature of the dust associated with ΔI_{100} to $9 < T_d < 15$ K.

The linear relationships between ΔI_{100} and the column density estimates A_B and $N(^{13}CO)$ (Figs. 4 and 5) suggest that the temperature of the dust must be constant over a large fraction of the volume sampled by ΔI_{100}. The flattening of the relationship between ΔI_{100} and A_B at $A_B > 5$ mag (Fig. 4) suggests that the temperature should drop at high opacities. In L183, the emission of ^{13}CO is optically thick in the core region where densities in excess of 10^4 cm^{-3} have been observed (Swade 1989). From the linearity between ΔI_{100} and $N(^{13}CO)$ (Fig. 5*b*) it is therefore inferred that ΔI_{100} must probe a limited density regime. By integrating ΔI_{100} over the area of L134 (340 Jy in 0.19 deg^2), assuming spherical symmetry, and using equation (5b) we derive an average density of $\langle n(H_2) \rangle = 1.7 \times 10^3$ cm^{-3}. This number is consistent with estimates of the average density from 6 cm H_2CO in L134 (about 10^3; Clark & Johnson 1983) and from ^{13}CO in L183 (1.2×10^3 cm^{-3}; Snell 1981), but lower than the estimated density in the core region of L134 [$n(H_2) > 5 \times 10^3$; Mattila et al. 1979]. It is surprising that the relationship between ΔI_{100} and $N(^{13}CO)$ is observed to be linear when one considers the physically different mechanisms altering the molecular and infrared emission.

4.2. *Grain Properties*

Even though only an upper limit can be derived for the mass absorption coefficient, our estimate (7) provides a valuable constraint since past determinations of C_{100} were hampered by large uncertainties. A reliable determination of the mass absorption coefficient is a prerequisite for mass estimates from infrared observations. The proximity of the upper limit of C_{100} to the empirical value given by Hildebrand (1983) and to the values predicted by Mathis & Whiffen (1989) who derive $C_{100} = 2$ g cm^{-2} and Draine & Lee (1984) who derive $C_{100} = 3.6$ g cm^{-2}, indicates that the actual temperature of the dust must be close to the limits presented in (4).

As suggested by Wright (1987, 1989), grains with high surface-to-volume ratios such as fractal or needle-shaped particles could have mass absorption coefficients that are orders of magnitude smaller than spherical particles of similar composition. Because of the consistency of C_{100} with the theoretical predictions which assume that the particles are roughly spherical,[2] we infer from our observations that there is no strong evidence that the bulk of the mass of the dust is contained in particles with shapes much different from spheres. We note that particles with a high surface-to-volume ratio are not strictly excluded by our limits since a temperature as low as 9 K implies $C_{100} = 0.008$.

The absence of nearly all of the cirrus emission in the map of ΔI_{100} demonstrates that the 60–100 μm ratio in the cloud complex is very constant except for the dense regions. In the following paragraphs we discuss the possible mechanisms causing the 60–100 μm variations.

The inferred variation in the infrared spectral distribution rules out the assumption that both the 60 and 100 μm emission are caused by one type of (classical) grain. Considering one grain component and assuming $Q_{abs} \propto \lambda^{-1}$, $\Theta = 0.21$ corresponds to a temperature $T_d = 26$ K. Since the energy absorbed by a classical grain is proportional to T_d^{4+1}, the change in the total energy density of the radiation field required to explain the infrared variations in the transition layer of the cloud is $(26/15)^5 > 15$. This could be achieved by an increase in column density equivalent to $A_V > 3$ mag in the radial direction in the narrow transition region. Such a contrast is inconsistent with the observations of L134 presented in Figure 4 where the decline in 60 μm emission can occur at $A_B < 2$ mag. It is also inconsistent with the properties of L1780 (Fig. 1*c*) which has a maximum total extinction $A_V < 4$ mag (Mattila 1979).

Also, the variation cannot be explained by assuming one grain component that undergoes a modification of properties in the transition region. Under this assumption of a single grain component responsible for both I_{60} and I_{100}, the 60–100 μm color can be used to derive the actual grain temperature. From the observed ratios we infer that a change in optical properties must cause the temperature to drop from 26 to 15 K. Considering equation (6) and assuming $I_{100}/A_B = 10$ MJy sr^{-1} mag^{-1} for the diffuse regions, the mass absorption coefficient should change from $C_{100} = 88$ g cm^{-2} in the outer regions to 4.6 g cm^{-2} in the 60 μm deficient regions. It can be shown that

$$C_{100} = [V/\sigma] Q_{abs}^{-1} \rho [M_{gas}/M_{dust}] = \tfrac{4}{3}[a/Q_{abs}] \rho [M_{gas}/M_{dust}] , \quad (8)$$

where V is the volume of a grain, σ is the geometrical cross section, and ρ is the specific gravity of the grain material. The last part of equation (8) is only valid for spherical particles where the ratio a/Q_{100} is independent of size (Hildebrand 1983). Relation (8) illustrates that strong variations in C_{100} must either be due to a change in the volume-to-surface ratio of nonspherical grains or to a change in the gas-to-dust ratio. Accretion of gas onto dust grains is the only mechanism that might lower the gas-to-dust ratio. However, it is improbable that this mechanism could lower the gas-to-dust ratio by one order of magnitude. Coagulation of grains could decrease the volume-to-surface ratio, but, as we shall argue below, the time scale for coagulation is too long to explain the sudden drop in temperature.

Our observations support the conclusion reached by several other studies in which the 60 μm emission is due to a separate grain component. The emission in the 100 μm band is assumed to be predominantly due to the classical grains. The physical mechanism causing the 60 μm emission is still subject to debate: a number of studies propose a grain component in which the grains show fluctuating temperatures (Draine & Anderson 1986; Désert, Boulanger, & Puget 1990), an alterna-

[2] This includes cylinders and spheroids. Mathis & Whiffen (1989) obtained the optical constants for porous composite grains. The extinction properties of these grains were derived from general Mie theory and applying a factor that describes the amount of vacuum in a grain. Such a treatment does not introduce the effects due to a large surface-to-volume ratio as suggested by Wright (1987).

tive explanation is provided by radiation from small particles at a constant high temperature such as pure iron particles (Chlewicki & Laureijs 1988) or graphite particles (Chlewicki 1987; Mathis & Whiffen 1989). In any case, the 60 μm emission involves small particles with radii less than 100 Å. Observations of high-latitude clouds suggest that these grains are different from the ones causing the emission in the *IRAS* 12 μm band (Laureijs et al. 1989).

The hypothesis of two grain components can account for the independent behavior of the two wavelength bands in the center of the cloud but fails to explain the sudden absence of the 60 μm emission. As argued by Chlewicki & Laureijs (1988) and Désert et al. (1990), observations of medium opacity clouds ($A_V < 3$ mag) indicate that the 60 μm carriers should absorb not only at UV wavelengths, but also substantially in the visual like the classical grains. This property prevents strong variations from occurring in the ratio I_{60}/I_{100}. Therefore, similar to the case of a single-grain component, the stepwise variation in the 60 to 100 μm ratio is difficult to explain in terms of only fixed grain components and variations in radiation field. To illustrate this point we have computed the emission at 60 and 100 μm from a homogeneous spherical dust cloud with a total center extinction of $A_V = 6$ mag. The emission properties of the grains were taken from Chlewicki & Laureijs (1988). Details of the computation can be found in Laureijs et al. (1989). In Figure 6 the results of the model have been plotted together with the observations of L134. The model shows a reasonable fit to the observed I_{100} (Fig. 6*a*) although it cannot match the observed linearity between I_{100} and A_B over the entire range of extinction. It provides an adequate fit to the constant level in ΔI_{100} for $A_B < 2$ mag, but fails to match the remaining data. The discrepancy in Figure 6*b* is due to too much predicted 60 μm emission in the inner parts of the cloud. The model can explain the constancy in I_{60}/I_{100} in L1780 (see Fig. 1*c*) but again fails to match the sudden drop.

The most probable explanation for the sudden drop in the 60–100 flux ratio is a change in the overall properties of the 60 μm grains in a narrow transition region. There are two mechanisms which could cause the modification: (1) coagulation due to grain-grain collisions depleting the amount of carriers, and (2) accretion of atoms by gas-grain collisions leading to formation of a "dirty ice" mantle altering the thermal and optical properties of grains. Since the variation in I_{60}/I_{100} occurs in a narrow transition region, the timescale of the process must be sufficiently small. The typical velocity dispersion in L134 and L183 outside the very dense regions is 1 km s^{-1} (Clark & Johnson 1983; van der Werf, Goss, & Vanden Bout 1988). Assuming a thickness of 5′ for the transition region we estimate a time-scale of $t \sim 1.4 \times 10^5$ yr. Draine (1985) showed that the time scale to deplete small particles by grain-grain collisions is in excess of 10^6 yr, whereas the time scale for gas-grain collisions is 10^5 yr, one order of magnitude smaller. For instance, consider a carbon grain of 50 Å in diameter. The time to accrete a water ice mantle of 10 Å thickness requires 2.8×10^4 yr, assuming a density of 10^3 cm^{-3} and gas temperature of 10 K (Spitzer 1978). The mantle increases the heat capacity of the grain preventing the temperature of the grain from fluctuating. The mantle also alters the overall optical properties of the grain into that of a typical refractory material. Only 7% of the cosmic abundance of oxygen is necessary if we assume that as much as 20% of all carbon is contained in 50 Å grains. Thus the formation of thin mantles can readily explain the sudden drop at 60 μm.

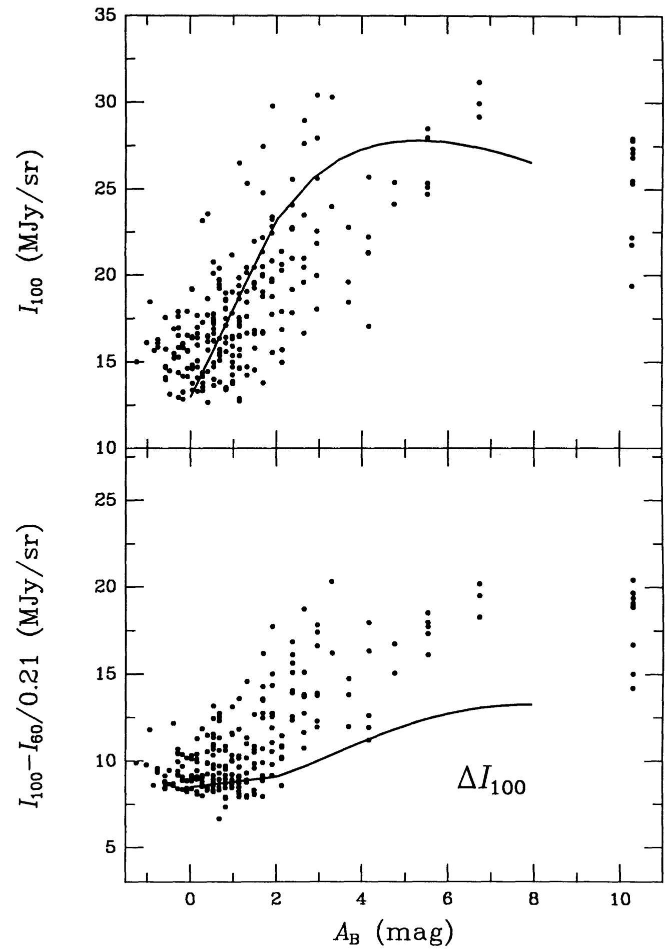

FIG. 6.—Similar to Fig. 4. The solid lines are obtained from a two-component grain model using a grain model with fixed composition. The model cloud is homogeneous and spherical, with a total extinction in the center of $A_V = 6$ mag ($A_B = 7.9$ mag).

The narrow transition layer also imposes that the reverse process, destruction of the mantle as soon as the particle drifts out of the cloud into the diffuse medium, must occur sufficiently rapidly. The most plausible mechanism is photodesorption of single molecules by energetic photons.

5. SUMMARY AND CONCLUSIONS

IRAS images of the L134 complex of dark clouds revealed extended regions where the 60 μm emission is very low with respect to the 100 μm emission. The 60–100 μm flux ratio has a constant value of 0.2 in the outer diffuse parts of the clouds but suddenly drops to less than 0.03 in the opaque cloud centers. By using a geometrical model we have shown that the drop occurs in a narrow transition layer that has not been resolved by *IRAS*. The observations provide direct evidence for dust temperatures colder than 15 K in dark clouds. This very cold dust component has been invoked in model computations of molecular clouds by Mathis et al. (1983) but has never been observed directly. The 15 K upper limit can be used to predict the minimum intensity of dust emission at wavelengths longer than 100 μm in dark clouds.

We have defined 60 μm deficient regions using the quantity $\Delta I_{100} = I_{60}/\theta$, where θ is the ratio I_{60}/I_{100} in the diffuse parts of the complex. The images of ΔI_{100} are free from diffuse cirrus emission down to a brightness level of 1 MJy sr^{-1}. We have found that ΔI_{100} is highly proportional to extinction and ^{13}CO column density. The relationships indicate that the temperature of the dust must be constant over a large fraction of the volume sampled by ΔI_{100} and that ΔI_{100} samples a limited density regime of order $n(H_2) \approx 10^{-3}$ cm^{-3}. These results show that the *IRAS* observations offer a method to separate the diffuse component from the intermediate density component in clouds without strong internal heating sources. The method is robust because it involves the subtraction rather than division of two maps.

The sudden drop of the 60–100 ratio in a narrow transition layer can be explained by assuming (1) two grain components emitting separately in the 60 and 100 μm bands, and (2) a change in the emission properties of the 60 μm grains in the transition layer. We have argued that the most likely mechanism for (2) is the accretion of a thin mantle of dirty ice onto the grains. Higher resolution observations of the transition region at mid-infrared wavelengths could provide an improved understanding of the grain component causing the variations in the 60 μm band. They could also test the hypothesis of the formation of grain mantles.

We have determined a firm upper limit for the mass absorption coefficient at 100 μm (7) which can be employed to constrain dust models. Since the clouds L134 and L183 have sizes comparable to the beam of the DIRBE instrument of *COBE*, the present data combined with *COBE* observations at $\lambda > 100$ μm should provide an accurate determination of the mass-absorption coefficient for regions in clouds with intermediate densities [$n(H_2) \sim 10^3$–10^4 cm^{-3}].

The research described in this paper was carried out by the Jet Propulsion Laboratory, California Institute of Technology, and was sponsored by The National Research Council and NATO through an agreement with the National Aeronautics and Space Administration. Work done at JPL was through the Astrophysics Division of NASA's Office of Space Science and Applications. R. J. L. acknowledges support of a Research Associateship administered by the National Research Council. F. O. C. was partially supported by NATO grant 0093/88 and NASA grant 055-89 at the University of Kentucky. T. P. acknowledges a grant from the Finnish Academy of Sciences. We are grateful to G. Helou and C. J. Lonsdale for critical reading of the manuscript.

REFERENCES

Bachiller, R., & Cernicharo, J. 1986, A&A, 166, 283
Benson, P.J., & Myers, P. C. 1989, ApJS, 71, 89
Bohlin, R. C., Savage, B. D., & Drake, J. F. 1978, ApJ, 224, 132
Boulanger, F., & Pérault, M. 1988, ApJ, 330, 964
Chlewicki, G. 1987, A&A, 181, 127
Chlewicki, G., & Laureijs, R. J. 1988, A&A, 207, L11.
Clark, F. O., & Johnson, 1983, ApJ, 247, 104
Cox, P., Krügel, E., & Mezger, P. G. 1986, A&A, 155, 380
Cox, P., & Mezger, P. G. 1989, A&A Review, 1, 49
de Boer, K. S., Lenhart, H., van der Hucht, K. A., Kamperman, T. M., Kondo, Y., & Bruhweiler, F. C. 1986, A&A, 157, 119
Désert, F.X., Boulanger, F., & Puget, J. L. 1990, A&A, 237, 215
Dickman, R. L., & Herbst, W. 1990, ApJ, 357, 531
Draine, B. T. 1985, in Protostars and Planets II, ed. D. C. Black, & M. S. Mattews (Tucson: Univ. of Arizona Press), p. 621
———. 1990, in The Interstellar Medium in Galaxies, ed. H. A. Thronson, & J. M. Schull (Dordrecht: Kluwer), in press
Draine, B. T., & Anderson, N. 1985, ApJ, 292, 494
Draine, B. T., & Lee, H. M. 1985, ApJ, 285, 89
Goldsmith, P. F. 1987, in Molecular Clouds in the Milky Way and External Galaxies, ed. R. L. Dickman, R. L. Snell, & J. S. Young (Berlin: Springer), p. 1
Goldsmith, P. F., & Langer, W. D. 1978, ApJ, 222, 881
Franco, G. 1989, A&A, 223, 313
Heiles, C., Reach, W. T., & Koo, B. C. 1988, ApJ, 214, 347
Heithausen, A., & Mebold, U. 1989, A&A, 214, 347
Hildebrand, R. H. 1983, QJRAS, 24, 267
Keene, J. 1981, ApJ, 245, 115
Kester, D. 1989, Manual for IMAGE 2, IPAC internal report
Laureijs, R. J., Chlewicki, G., & Clark, F. O. 1988, A&A, 207, L11
Laureijs, R. J., Chlewicki, G., Clark, F. O., & Wesselius, P. R. 1989, A&A, 220, 226
Laureijs, R. J., Mattila, K., & Schnur, G. 1987, A&A, 184, 269
Lee, M. H., & Rogers, C. 1987, ApJ, 317, 197
Low, F. J., et al. 1984, ApJ, 278, L19
Mathis, J. S., Mezger, P. G., & Panagia, N. 1983, A&A, 128, 212
Mathis, J. S., & Whiffen, G. 1989, ApJ, 341, 808
Mattila, K. 1979, A&A, 78, 253
———. 1986, A&A, 160, 157
Mattila, K., Winnberg, A., & Grasshoff, M. 1979, A&A, 78, 275
Myers, P. M., & Benson, P. J. 1983, ApJ, 266, 309
Savage, B. D., & Mathis, J. M. 1979, ARA&A, 17, 73
Snell, R. L. 1981, ApJ, 45, 121
Snell, R. L., Langer, W. D., & Frerking, M. A. 1982, ApJ, 255, 149
Spencer, R. G., & Leung, C. M. 1978, ApJ, 222, 140
Spitzer, L. 1978, Physical Processes in the Interstellar Medium (New York: Wiley) p. 207
Swade, D. A. 1989, ApJ, 346, 828
Terebey, S., & Fich, M. 1986, ApJ, 309, L73
Ungerechts, H., Walmsley, C. M., & Winnewisser, G. 1980, A&A, 88, 259
van der Werf, P. P., Goss, W. M., & Vanden Bout, P. A. 1988, A&A, 201, 311
Werner, M. W., & Salpeter, E. E. 1969, MNRAS, 145, 249
Whittet, D. C. B., & van Breda, I. G. 1979, MNRAS, 192, 467
Wright, E. L. 1987, ApJ, 320, 818
———. 1989, ApJ, 346, L89